PHYSICAL REVIEW A **94**, 022712 (2016)

Water fragmentation by bare and dressed light ions with MeV energies: Fragment-ion-energy and time-of-flight distributions

W. Wolff* and H. Luna
Departamento de Física, Universidade Federal do Rio de Janeiro Caixa Postal 68528, Rio de Janeiro, 21945-970, RJ, Brazil

R. Schuch
Department of Physics, Stockholm University, Alba Nova University Center, SE-106 91 Stockholm, Sweden

N. D. Cariatore and S. Otranto
IFISUR, Universidad Nacional del Sur, CONICET, Departamento de Física, Bahía Blanca, Argentina

F. Turco, D. Fregenal, G. Bernardi, and S. Suárez
Centro Atómico Bariloche, Bustillo 9500 - San Carlos de Bariloche, Río Negro, Argentina
(Received 22 March 2016; revised manuscript received 5 July 2016; published 22 August 2016)

The energy and time-of-flight distributions of water ionic fragments produced by impact of fast atoms and bare and dressed ions; namely, H^+, Li^{0-3+}, C^{1+}, and C^{2+} are reported in this work. Fragment species as a function of emission energy and time-of-flight were recorded by using an electrostatic spectrometer and a time-of-flight mass spectrometer, respectively. An improved Coulomb explosion model coupled to a classical trajectory Monte Carlo (CTMC) simulation gave the energy centroids of the fragments for the dissociation channels resulting from the removal of two to five electrons from the water molecule. For the energy distribution ranging up to 50 eV, both the experiment and model reveal an isotropic production of multiple charged oxygen ions, as well as hydrogen ions. From the ion energy distribution, relative yields of the dissociation resulting from multiple ionization were obtained as a function of the charge state, as well as for several projectile energies. Multiple-ionization yields with charge state up to 4+, were extracted from the measurements of the time-of-flight spectra, focused on the production of single and multiple charged oxygen ions. The measurements were compared to ion-water collision experiments investigated at the keV energy range available in the literature, revealing differences and similarities in the fragment-ion energy distribution.

DOI: 10.1103/PhysRevA.94.022712

I. INTRODUCTION

In the last few decades, the irradiation of malignant tumors by high-energy protons and carbon ions is considered as a standard treatment in cancer therapy. Ion-beam therapy strongly relies on a detailed characterization of the damage caused by energetic ion impact on the medium, including the water molecule. Most of the ion energy deposited in the tissue along the ionization tracks are absorbed by water molecules, leading to the ejection of electrons and the formation of neutral and charged fragments. Those secondary species will contribute to the biological damage, in the vicinity of DNA, competing in importance with single and double direct breaks of DNA strands. The action of those secondary species in the medium is frequently referred to in the literature as the radiolysis of water molecules [1–3]. In this context, it is relevant to point out that a more effective fragmentation yield of the water molecule does not necessarily occur at the Bragg peak, where the known linear energy transfer (LET) is maximum. Furthermore, in the distal region of the Bragg peak the number of primary ions produced in water ionization induced by C projectiles is almost flat in relation to the maximum of the Bragg peak [4].

These regions lie within the intermediate-energy range of few MeV/u to keV/u. There, the water radiolysis is strongly related to the energy distribution of the ejected ionic and neutral fragments. The ion-fragments include the lightest fragment-ion, H^+, plus the heavier OH^+ and O^{q+} ions [4–8]. For carbon projectiles, the energy region of interest ranges from a few keV up to ∼3 MeV, with charge states from 0 to 2+ [4].

Ionization of water molecules leading to the removal of two or more electrons is followed by molecular dissociation [9,10]. For double electron removal, three main pair-ion fragmentation channels compete in importance; namely, $H^+ + H^+ + O$, $H^+ + OH^+$, and $H + H^+ + O^+$. For ionization of higher degrees, the dominating fragmentation pathways can involve three-body breakups of the water molecule: $H^+ + H^+ + O^+$, $H^+ + H + O^{q+}$, and $H^+ + H^+ + O^{q+}$, with $q \geqslant 2$.

Although there are in the literature several studies concerning the influence of the velocity and charge state of the projectile on the dissociative ionization of water molecule, a detailed knowledge of general features of the dissociation pattern leading to the formation of multiply charged ion pairs remains scarce, in particular in the intermediate-energy range. The dissociation channels of multiply ionized water have been studied experimentally and/or combined with theoretical calculations for slow- [11–20] and fast-ion impact [21–33] with single and doubly charged projectiles [10–14,21–26,30,34,35] and multicharged ions [3,20,27–29,31,32]. Slow collisions are considered in the energy range of tens of keV/u to a few MeV/u.

The focus of this work is on the experimental and theoretical energy distributions of ionic fragments originating from

*wania@if.ufrj.br

ion-water (atom-water) collisions, emitted at several angles relative to the direction of the projectile beam (H^+, Li^{0-3+}, C^{1+}, and C^{2+}). To identify masses and charges of the charged fragments, an analysis based on a time-of-flight spectroscopy was used to discriminate contributions of ionic species. Two-body and/or three-body dissociation probabilities have been predicted in a theoretical calculation based on the Coulomb explosion (CE) framework and Monte Carlo simulations. These calculations were used as a guide to link the measured fragment-ion energy distributions with the final dissociative states of the molecule. The study of the parent molecule ion H_2O^+ and single ionized dissociation channels such as $(H + OH^+)$, $(H^+ + H + O)$ and $(H + H + O^+)$ were not the focus of this work.

It is worth mentioning that one of the goals of the present report is to shed light onto processes which lead to the production of highly charged oxygen fragments O^{q+}. Nevertheless, it is also important to correlate the charge state of the transient water molecule prior to dissociation with the ejected ion species, in particular the hydrogen ions, which can acquire a broad range of energies from eV to tens of eV with their abundances varying by orders of magnitude. In this particular subject, the bare ions (H^+ and Li^{3+}) were used as a benchmark in the comparison with other dresses ions, Li^+, C^+, Li^{2+}, C^{2+}, to study the role of projectile screening in the molecular dissociation.

The paper is organized as follows: The two experimental methods are described in Sec. II. In Sec. II A the procedures using the electrostatic spectrometer to record electron- and ion-energy distributions are given. Then, in Sec. II B, details are provided on the operation of the spectrometer as a time-of-flight mass spectrometer. In Sec. III the description of the theoretical approach is presented, based on the n-body classical trajectory Monte Carlo simulation combined with a Coulomb explosion model.

Section IV A starts with a discussion of the profile of the H^+ energy distributions. Features of the structures observed in the distributions belonging to the fragmentation channels are addressed and partial yields are obtained that explore the channel intensities due to action of different projectile ions. Section IV B presents the partial yields of multiple ionization induced by distinct projectile ions, extracted from the time-of-flight spectra. The energy transfer to single and multiple charged fragments are included in the investigation, depicting the strength of the fragmentation process. The conclusion section summarizes the results and proposes an extension of the investigation in order to obtain absolute cross sections.

II. EXPERIMENTAL METHODS

The experiments were carried out at the 1.7 MV pelletron accelerator facility of the Centro Atómico Bariloche [36]. Briefly, H^+, $Li^{q'+}$, and $C^{q'+}$ beams (q' denotes the charge state of the projectile ion) with energies varying from keV/u to MeV/u were obtained and selected by a switching magnet and subsequently directed towards the projectile-target collision beam line. The accelerator energy range suited well this investigation.

The base pressure in the beam line and in the collision chamber are maintained at 4×10^{-7} mbar. During the experiment the working pressure in the collision chamber was raised and kept around 1.5×10^{-6} mbar. The water target is stored in a glass vial and degassed by several thaw-pump cycles, eliminating mostly air contaminants. It is sublimated at room temperature and the vapor is injected through a 0.25-mm-diameter needle as an effusive gas jet into the interaction region. The target density is regulated by an all-metal precision leak valve. The beam current of all projectile species used in this work is measured at the end of the beam line by a biased Faraday cup, with typical beam currents of 10–70 nA.

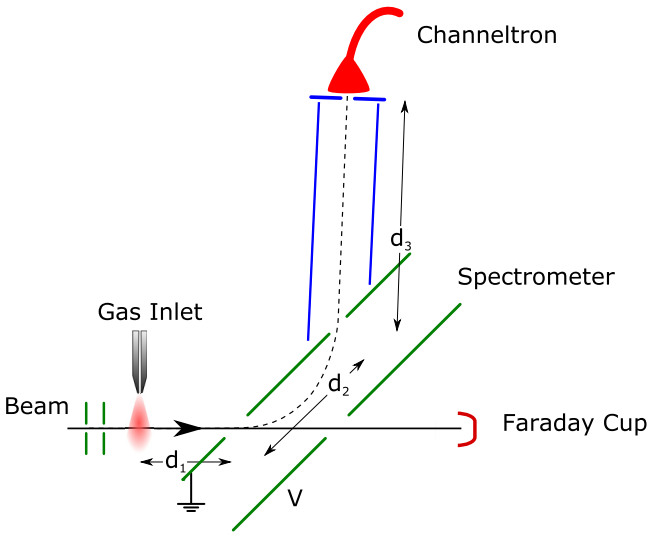

FIG. 1. Scheme of interaction region and main experimental components used for collecting the fragment ions from the target. Combined electrostatic and time-of-flight spectrometer is shown, where the distances d_1, d_2, and d_3 traveled by the fragment ions are indicated by the dotted line and the beam trajectory is indicated by the solid line.

The experimental chamber is equipped with an electrostatic cylindrical mirror spectrometer [36]. The axis, defined by two slits, forms an angle of 42.3 degrees with the direction of the incident projectile beam. The spectrometer and an electron multiplier (channeltron) detector were used for collection and detection of electrons and positive charged fragments. By varying the homogeneous electric field created between the cylinders normalized in energy steps to the same pre-fixed collected charge, a range of selected electron or ion energies can be measured. The scheme of the interaction region and the main experimental components are illustrated in Fig. 1.

A. Total fragment energy distributions

The experimental procedures followed several steps. First, the electron energy distribution was measured at zero degrees respective to the incident beam ensuring the transmission of only one selected projectile species and determining precisely its incident energy. In this step a four-jaw slit collimator, inserted before the collision chamber, was adjusted in order to avoid beam contamination and for positioning and alignment of the beam in the interaction region, as well as for defining the collision area of 0.64 mm^2. The operation of the spectrometer, as well as the signal and data processing, is described in detail

in Ref. [37]. Afterwards, without changing any parameters, the voltages at the spectrometer were changed to collect positive fragment ions. The total-fragment-energy distributions for several angles of emission with respect to the beam direction from 10 up to 170 degrees were recorded. These distributions were measured as a function of the energy per charge q of the fragment ions. The spectra were taken in 0.5 eV steps. The intensities were corrected for the transmission function of the spectrometer (i.e., intensities divided by E/q). The spectra exclude thermal ions originated from molecule ionization with or without dissociation, therefore single ionization cannot be measured with this method.

Structures are clearly discerned in the energy spectra revealing the contribution of different fragmentation channels of the water molecule. Nevertheless, some of the structures in the energy distributions arise from overlap of ions from adjacent fragmentation channels. Additionally, it is possible to have overlap of spectral structures of multiple charged ions when the energy-to-charge ratios are similar. The present setup cannot provide qualitative as well as quantitative results below 2 eV/q due to resolution and efficiency collection of the ions.

To verify the calibration of the spectrometer, measurements with other molecular targets such as H_2, CO_2, and CH_4 were done and the energy distribution structure was compared with the literature (H_2 [38–40], CO_2 [41,42], CH_4 [43]). The structures are in good agreement with the spectral distributions found in the literature.

B. Time-of-flight mass spectra

To identify the charge and mass of each detected fragment we apply time-of-flight (TOF) mass spectroscopy. For these measurements the projectile beam is pulsed, in some cases at the injector of the pelletron accelerator, just at the entrance of the acceleration tube or, in other cases, after its exit in the transport beam line. The time-of-flight spectra were not sensitive to the choice of the pulsing beam location. The beam was pulsed with a fixed frequency of 10 kHz and a pulse width of 500 ns and deflecting voltages of +500 V and −500 V. Special care was taken to guarantee the beam-on and beam-off condition during the collecting of the time-of-flight spectra.

The coaxial cylindrical mirror spectrometer was used for obtaining the TOF spectra in a similar way as that applied in Ref. [44]. When the outer cylinder is set to a fixed potential, the energy per charge of the charged fragment is preset and only fragments with energies within the spectrometer resolution were guided from the collision region towards the detector (channeltron). A schematic drawing shown in Fig. 1 (not in scale) depicts the trajectory of the selected charged fragment. The total path length traveled by the recoil ions toward the detector is given by the distances d_1 (186 mm), d_2 (527 mm), and d_3 (1125 mm). The initial recoil-ion velocity depends only on the released energy acquired by the fragments from the collision process. Note that the extracting voltage was not applied to collect the ions from the collision area.

The stop signal for the Time-to-Amplitude-Converter and the trigger for data acquisition were obtained from the pulsed beam circuitry, while the start signal was obtained from the first fragment ion detected by the electron multiplier detector. The ion signals were amplified by a fast pre-amplifier. Both signals were standardized by constant fraction discriminators, and the stop signal was delayed by 30–70 μs. The delay time was set depending on the selected fragment-ion energy per charge. The TAC spectra were recorded and normalized to a preselected total beam charge, which was obtained by integrating the current measured by the Faraday cup. The beam current in this mode was kept around 0.1–0.6 nA.

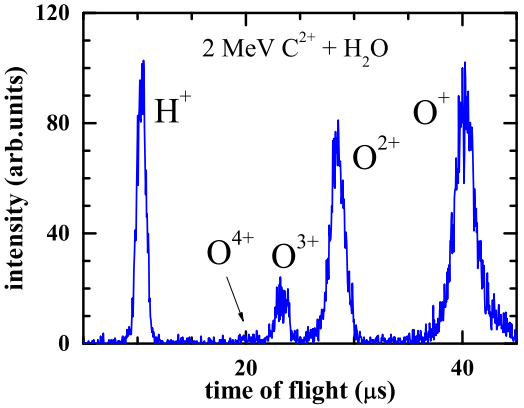

FIG. 2. Time-of-flight spectrum recorded for 2 MeV C^{2+} ion beam at the detection angle of 10 degrees. Only fragment ions of O^{q+}, with q from 1+ to 4+, and H^+ with 2 eV/q are measured.

Figure 2 shows a typical TOF spectrum recorded in the interaction of C^{2+} with water, setting the electrostatic analyzer to accept fragment ions within a preset energy per charge of 2 eV/q and for a detection angle of 10 degrees. It shows H^+ and up to fourfold charged oxygen ions, O^{q+}. Note that, with the present experimental setup, the individual contributions of O^+ and OH^+ cannot be separated and the TOF of both fragments should coalesce to the same peak (see Fig. 2). However, the contribution of fragments with small release energies from channels (H, H, and O^+) and (H and OH^+) can be disregarded due to the their low collection efficiency. The same argument applies to the missing H_2O^+ ions emitted with thermal energies.

III. THEORETICAL MODEL

To provide a theoretical insight into the kinetic-energy spectra of ionic fragments, n-body classical trajectory Monte Carlo (n CTMC) simulations [45] have been conjugated with a Coulomb explosion model. In this n CTMC model, the water molecule is represented by a single center model in which eight electrons are sorted with sequential binding energies. The interaction between the electrons and the dominant element of the molecule (oxygen) is represented by the Garvey potential [46]

$$V(r) = \frac{(N-1)[1-\Omega(r)] - Z}{r}, \tag{1}$$

$$\Omega(r) = [(\eta/\xi)(e^{\xi r} - 1) + 1]^{-1}. \tag{2}$$

The corresponding parameters are $Z = 8$, $N = 8$, $\xi = 1.36$, $\eta = 2.41$. According to this potential, the target electrons see a charge +8 when they are near the oxygen nucleus while they experience the asymptotic charge +1 at large distances. Throughout the collision, the position of the projectile-target

nucleus saddle potential is tracked at all times. Each electron that is removed from the target is considered to be emitted at the precise instant that it crosses the projectile-target nucleus saddle for the last time. Moreover, the position and momenta of the projectile are recorded whenever an electron crosses the potential saddle leaving the target region. By so doing, a nonarbitrary criterion is introduced to determine, for each multiple capture and/or ionization event, the geometrical configuration of the collision system to be used to initialize the Coulomb explosion dynamics.

In a second stage, a Coulomb explosion (CE) simulation proceeds. In this CE model the ionic fragments are explicitly considered and assumed to be at rest, still under the bonding length and angle of the neutral H_2O molecule. Furthermore, the H_2O molecule is assumed to be randomly oriented. The CE model is fed event by event with the positions and momenta of the projectile and target nucleus center of mass recorded at the instant the last ionized or captured electron crossed the potential saddle. The Coulomb explosion is then simulated by numerically solving Hamilton's equations for all ionic fragments plus the projectile. The total number of events recorded for n-electron capture or ionization are used for each of those fragmentation channels corresponding to n-electron removal. Advantages of the present combined model, hereafter referred to as CE-CTMC, are that the Coulomb explosion dynamics are initialized considering the projectile's position and momentum at the time that the n-electron removal (via ionization, charge-exchange, or transfer-ionization mechanisms) takes place. Since such removal can be reached either in the incoming or outgoing phases of the projectile trajectory, CTMC provides a nonarbitrary route to initialize our CE model with post-collisional interaction (PCI) over a wide energy range.

As already pointed out by Siegmann *et al.* [32], one of the most difficult fragmentation channels to describe by a CE model is $H_2O \rightarrow H^+ + OH^+$. The unrealistic approximation of OH^+ by a point charge located somewhere between the H and O nuclei leads to proton energies between 9 and 15 eV, which are larger than those measured by different laboratories which encompassed the range 4–7 eV. The incorporation of fractional charges [47,48] provides a route to diminish the asymptotic proton energies. However, our preliminary tests did not lead us to the expected energy range. In fact, this fragmentation channel can be reached in principle via three possible mechanisms: (i) direct double ionization, which leads to an asymptotic proton energy of 6.8–7.1 eV [12,32]; (ii) resonant capture or inner-shell ionization followed by Auger deexcitation (asymptotic proton energy of about 4.6 eV) [12]; and (iii) single ionization or capture followed by electron excitation to autoionizing states of (OH), which then decay to $(OH)^+$ (kinetic-energy release of about 2–6 eV) [49].

Our first step towards a more detailed description of these fragmentation mechanisms has been the exploration of functional forms for the interfragment potentials that would physically fit and bring proton energies into agreement with the data. In this sense, two semiempirical models have been employed at this stage. For mechanism (i) we considered that the proton interacts with the $(OH)^+$ complex via a Coulomb interaction seeing an effective charge at short distances which via exponential factors evolves into a +1 charge at large distances. Mechanisms (ii) and (iii), on the other hand, rely on the fact that they originate in a single ionization or capture process. Hence, an αr^{-2} dipole-type potential, which provides a rough approximation for a neutral environment, is used and switched into the same asymptotic Coulombic description of mechanism (i) by means of time-dependent exponential factors, $\exp(-\lambda t)$. The timescale for switching has been arbitrarily set to 5×10^{-15} s, which is typical for molecular rearrangements. In the following discussion, we refer to channels (ii) or (iii) as $H^+ + (OH)^*$, provided they lead to similar proton energies.

IV. RESULTS AND ANALYSIS

The following discussion is divided into two sections. The first section discusses the measurements of the total ion-fragment energy distributions using the electrostatic spectrometer. The measurements were carried out for several projectiles with different charge states and impact energies, colliding on H_2O. Second, the time-of-flight mass spectrometry technique is used to clarify the low-energy part of the energy distribution spectra.

Three projectile species were investigated; namely, proton, lithium, and carbon ions. The lithium species were selected due to the fact that all its charge states (neutral, dressed, or bare) could be delivered by the accelerator with energies that probe the water fragmentation at the intermediate-energy range of MeV/u. The proton case was particularly selected to be compared with the bare-lithium case at the same collision velocity. The partially dressed carbon ions, besides their importance in the study of molecular processes on radiation damage in cells, allowed a direct comparison with the dressed-lithium projectiles ($q' = 1$ and 2) to better understand the role of projectile effective charge in the molecular dissociation process. To the authors knowledge there is a lack of experimental and theoretical studies on this subject in the energy range of a few keV/u to MeV/u.

A. Electrostatic spectrometry results

In this section, the relative intensity of the energy distributions for several detection angles was analyzed for the water fragmentation occurring after collision with different projectiles. The main goal is to compare the effective role of projectile parameters, such as incident-energy per mass ratios and charge states, in the fragment-ion energy distribution. The relative intensity represents the fragment-ion production yield normalized to the number of projectiles and target pressure. The distributions are differential with respect to the detection angle and to the energy per charge state of the detected ion fragment. We start our discussion with the $Li^{q'+}$ projectiles with $q' = 1$, 2, and 3. Later we extend the analysis to partially dressed carbon-ion projectiles, $C^{q'+}$. The energy range studied in this work lies between 160 keV/u and ~1 MeV/u.

1. $Li^{q'+}$ projectiles

Figure 3(a) shows, for a fixed detection angle of 10 degrees, the energy distributions of H^+ fragments emitted by three different Li^{3+} projectile energies; namely, 1.6, 3.0, and 5.8 MeV. The three spectra show similar features presenting broad structures at low energies—around 5, 15,

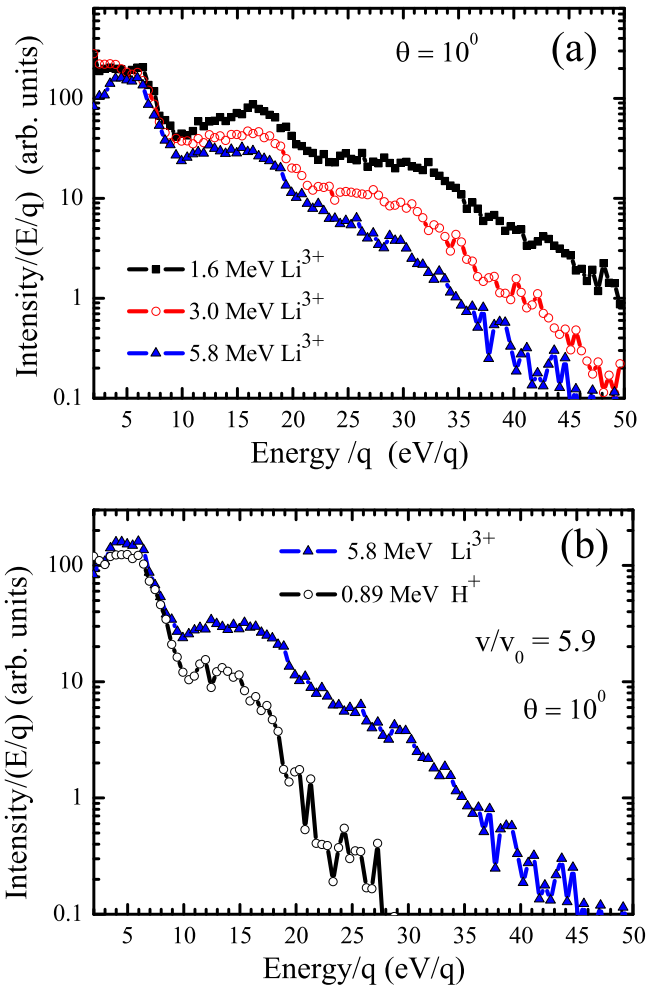

FIG. 3. Relative intensity of fragment-ion energy distributions (spectrometer transmission corrected) for bare ion projectiles colliding on water, differential in energy per charge of the fragment ions (eV/q). The emission angle is 10 degrees. (a) Li^{3+} at three energies: 1.6 MeV (black squares), 3.0 MeV (open red circles), and 5.8 MeV (blue triangles). (b) Li^{3+} and H^+ at the same velocity of $5.9v_0$ (5.8 MeV Li^{3+}, closed blue triangles) and 0.89 MeV H^+ (open circles).

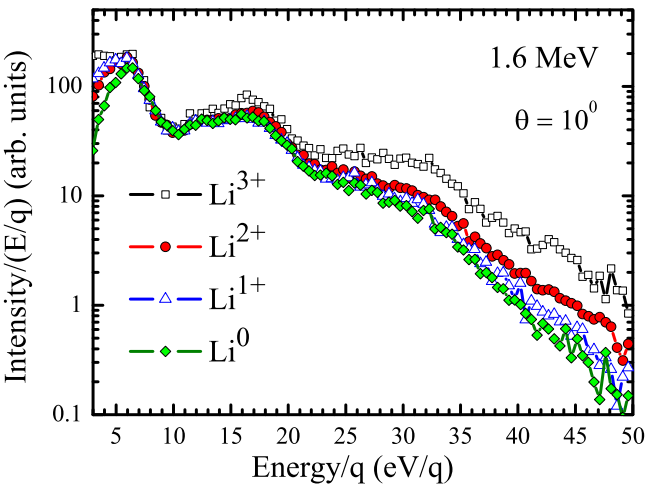

FIG. 4. Li^{0-3+} at 1.6 MeV: Li^0 (green closed diamonds), Li^+ (blue open triangles), Li^{2+} (red closed circles), and Li^{3+} (black open squares). The emission angle is 10 degrees.

and 25–30 eV. The main difference lies in the high-energy edge distribution, where the three projectile energies have different slopes in the general monotonic decrease trend (above 30 eV). Higher production of energetic H^+ ions occurs for lower projectile energies, where the double electron removal channels, in particular the electron capture with multiple ionization (transfer ionization), start to compete with the pure single-ionization channel [50,51].

This difference towards the high edge of the fragment energy distribution is also present when equivelocity bare ions, H^+ and Li^{3+}, are compared. The comparison is showed in Fig. 3(b) for $5.9v_0$ (v_0 being the Bohr velocity and at an emission angle of 10 degrees). In this case, the spectra become remarkably different for fragment energies above the 5 eV structure. At these projectile velocities, electron-capture and transfer-ionization channels can be disregarded for both projectiles. Therefore, the main contributions come from the pure single-, double-, and triple-ionization channels. The observed differences in the spectra can be explained in light of the q'^2 scaling rule, because at this velocity the perturbative collision regime is almost reached [51]. The result presented in Fig. 3(b) is partially in accordance with the work of Barros *et al.* [23], where the energy distribution of H^+ fragments ejected by 20–100 keV proton impact show the maximum yields centered at 9 and 15 eV.

In Fig. 4 the fragment-ion energy distribution is analyzed as a function of the charge state of the lithium projectile ($q' = 0$ to 3) for a fixed incident energy of 1.6 MeV and a detection angle of 10 degrees. It can be seen that the projectile charge states do not have an explicit major influence on the shape of the distribution. The fragment-ion distributions start to change for energies above 25 eV, showing an explicit correlation between the projectile charge state and the yield of energetic H^+ fragment production.

Nevertheless, linking the measured fragment-ion energy distribution with the final dissociative state of the molecule is not a straightforward task. Absolute pure ionization and electron-capture cross sections provide the dissociative channel which dominates the ionization process [51]. This information could furnish a hint on which dissociative channel(s) dominate(s) the total multiple ionization, but yet it cannot tell the final fragment-ion energy distributions.

In this work, the CE-CTMC model (described in Sec. III) is used as a guide to link the measured fragment-ion energy distribution with the final dissociative states of the molecule. As an example, the experimental data of the fragment-ion energy distribution for the 3 MeV Li^{3+}-H_2O collision is shown in Fig. 5 together with the theoretical analysis of CE-CTMC model. The calculation gives the final dissociative state of the molecule with the corresponding kinetic energy of the fast H^+ fragment. In this case the channel $H^+(O^+)H$ means that, around 14 eV, the structure is formed by a H^+ ion from the fragmentation channel $H^+ + O^+ + H$, where the O^+ and H fragments are not observed.

The calculation shown in Fig. 5 provides energy centroids for the channels listed in Table I.

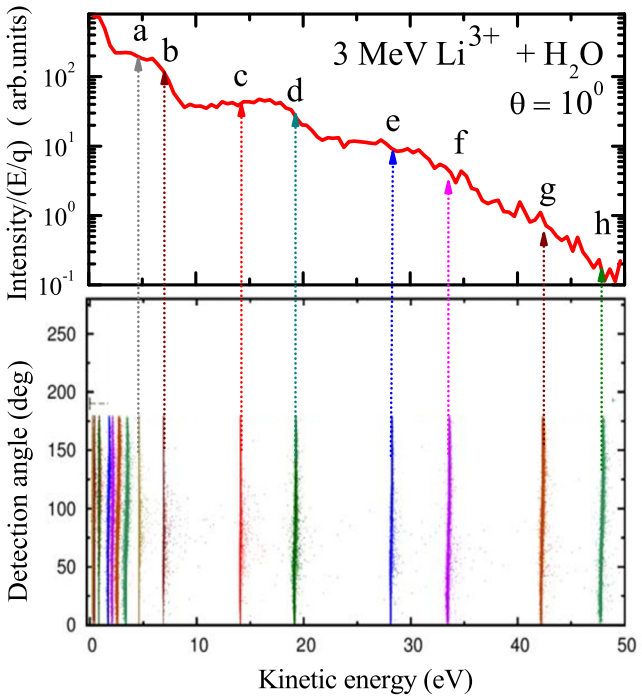

FIG. 5. (top) Experimental data of 3 MeV Li^{3+} colliding with H_2O at a detection angle of 10 degree. (bottom) Coulomb explosion (CE) model conjugated with CTMC calculations for the same collision system. The figure shows the detection angle as a function of the kinetic energy of several fragmentation channels. The designation of fragmentation channels are also included.

By taking the calculation procedure described in Fig. 5 as a guide, the experimental fragment-ion energy distributions were analyzed for lithium and carbon projectiles. The first conclusion is that the energy distributions would evidence contributions involving the removal of up to five electrons, with the higher kinetic energies of the H^+ fragments being related to the higher degree of ionization of the molecule. Double ionization of fragmentation channels a–c would lie in the 5–15 eV region, triple ionization associated with channels d and e in the 15–30 eV region, fourfold ionization associated with channels f and g in the 30–45 eV region, and fivefold ionization associated with te channel h in the 45–50 eV region. At low energies, around 2–5 eV, slow heavy fragments, mostly multiply charged oxygen ions, dominate. In this region, it is not possible to use the calculations to distinguish in the experimental distributions the different possible contributions of O^{q+} ions in relation to the less-energetic H^+ fragment ions.

TABLE I. Dissociative channels of H_2O^{q+}.

Label	Channel	Energy centroid (eV)
(a)	$H^+ + OH^*$	4.6
(b)	$H^+ + OH^+$	6.8
(c)	$H^+ + H + O^+$	14.1
(d)	$H^+ + H^+ + O^+$	19.1
(e)	$H^+ + H + O^{2+}$	28.1
(f)	$H^+ + H^+ + O^{2+}$	33.4
(g)	$H^+ + H + O^{3+}$	42.3
(h)	$H^+ + H^+ + O^{3+}$	47.7

To estimate the relative contribution of the different fragmentation channels we use a method based on a fitting procedure of trial peak functions (e.g., Gaussian functions). This procedure is presented in Fig. 6(a) for 1.6 MeV Li^+ projectiles at the detection angle of 10 degrees. The Gaussian functions were centered (fixed parameter) at the energy centroid predicted by the calculation. It was considered in the fitting procedure that the double ionization process, $(H^+ + OH^+)$, has a narrower distribution than the three-body distributions; a feature that is based on the measured kinetic energies of the H^+ fragments emitted in collisions with H^+ and He^{q+} projectiles of Ref. [12].

Figure 6(b) shows, for 1.6 MeV $Li^{q'+}$ ($q' = 0$, 1, 2, and 3), the relative intensities of the fragmentation channels (a-h) as function of the energy centroids obtained from the CE-CTMC calculation. The relative intensities are defined as the areas of the fit functions divided by the sum of all areas of all fragmentation channels. From this analysis it is possible to infer that, when the projectile charge state increases, the yield of higher degree of ionization channels $[(H^+ + H^+ + O^{q+})$ and $(H^+ + H + O^{q+})]$ also increases. It is important to point out that this is in accordance with measurements at the lower projectile energy of 21 keV $Ne^{q'+}$ with $q' = 3$, 5, and 9 [15]. For these lower projectile energies, transfer-ionization channels are expected to be as important as the direct single ionization [50,51].

Figure 6(c) shows the relative intensities of the fragmentation channels for the Li^{3+} projectile at three energies: 1.6, 3.0, and 5.8 MeV. The ratios show a general trend of decreasing contributions of higher ionization channels $(H^+ + H^+ + O^{q+})$ and $(H^+ + H + O^{q+})$ with increasing projectile energy. This observed feature is also corroborated by the absolute ionization-cross-section analysis of Ref. [51], which shows that, for higher Li^{3+} energies, the role of transfer ionization decreases in relation to single direct ionization.

For completeness we compare our results with previous work in the literature, although, to the authors knowledge, the data available do not cover the energy range studied in this work. As pointed out before, the MeV/u range covers the stopping-power maximum for heavy ions and is also the range in which the electron capture (plus transfer ionization) competes with pure ionization [50,51]. In slow He^{2+} on H_2O collisions (1–5 keV) [13–15], the measured fragment-ion energy distribution extends up to 30–35 eV, while the interaction of 21 keV Ne^{9+} [17] and 220 keV Xe^{22+} [18] at an observation angle of 135 degrees shows much more energetic H^+ ions with energies up to 70–80 eV. For impact of 450 keV Ar^{9+} and H^+ fragments from the (H^*,H^+, and O^{q+}) channel were measured with kinetic-energy release (KER) as high as 170 eV [28,29]. Their spectra also showed a clear correlation between the KER maximum peak at energies of 30, 50, 70, and 80 eV, and the oxygen ion fragment (O^{q+}) charge state $q = 1$, 2, 3, and 4, respectively. Werner *et al.* [30,31] measured the total KER distribution in the collision of 250 keV He^+. They obtained H^+ fragments with energies up to 60 eV, while for 92.4 keV O^{6+} and 126 and 742 keV O^{7+} ions the total KER values increased up to 130 eV. For fast projectiles, Siegmann *et al.* [32] measured

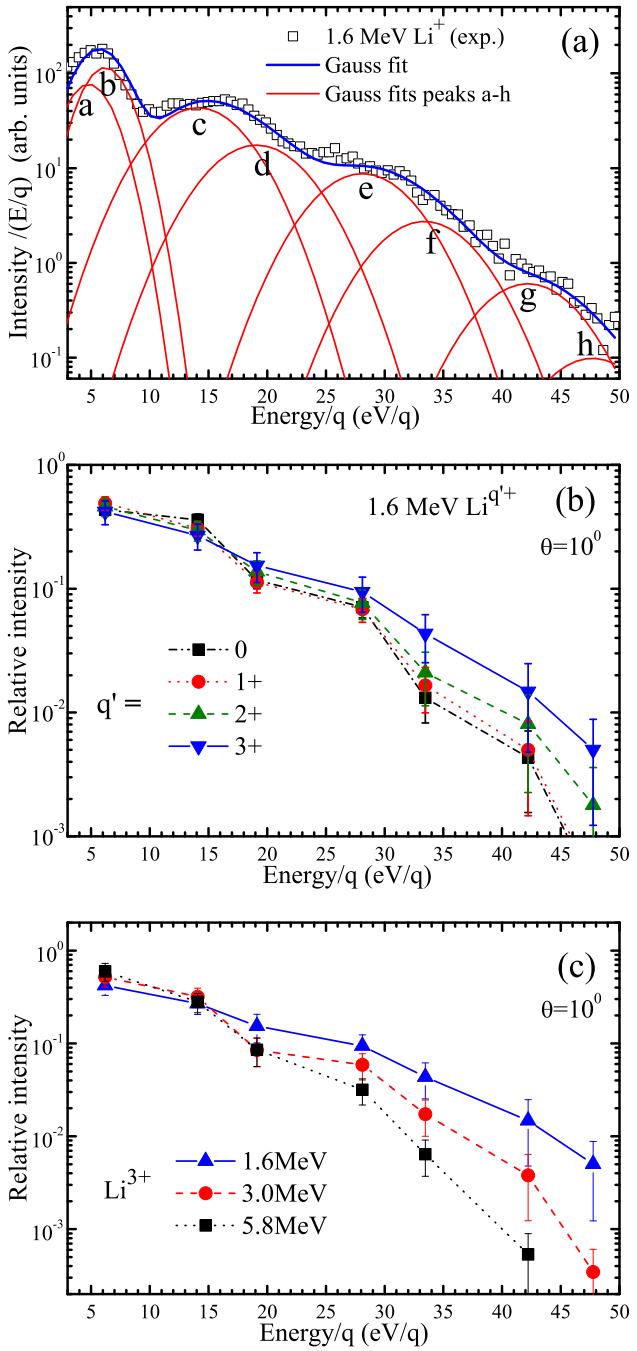

FIG. 6. (a) Intensities of the fragment ion as function of their energy per charge (eV/q), corrected for the transmission of the spectrometer. Experimental data: black open squares show Gaussian distributions (red lines) fit to fragmentation channels a–h centered at the energy centroid predicted by present CE-CTMC model. Blue line is the sum of the Gaussian distributions. (b) Relative intensities of fitted area to total area as function of the energy centroids for each fragmentation channel for 1.6 MeV $Li^{q'+}$ projectile: Li^0 (black closed squares), Li^+ (red closed circles), Li^{2+} (green closed upward triangle), Li^{3+} (blue closed downward triangle). (c) Relative intensities of fitted area to total area for each fragmentation channel as function of the energy centroids for each fragmentation channel for the Li^{3+} projectile at three energies: 1.6 MeV (black closed squares), 3.0 MeV (red closed circles), 5.8 MeV (blue closed upward triangles). Lines are to guide the eye.

a total KER for 5.9 MeV/u $Xe^{17,18,43+}$ projectiles for the fragmentation channels ($H^+ + OH^+$), ($H^+ + H^+ + O^+$), and ($H^+ + H^+ + O^{2+}$), finding their KER peaks centered around 7, 40, and 70 eV, but with their distributions extending up to 30, 100, and 140 eV, respectively.

2. $C^{q'+}$ projectiles

In hadron-therapy treatments, carbon ions have advantages over protons in providing a more defined and higher local dose deposition. As a consequence they allow a better control in irradiation of aggressive tumors and a lower acute or late toxicity. The energy deposition at the end of the ion trajectory of a carbon beam is larger than that of a proton beam, being the linear energy transfer confined into a narrower Bragg peak [52]. Many electron tracks are produced that cause locally multiply damaged sites within the DNA. When a large amount of breaks on the chemical links occur, even double-stranded DNA break by one hit, DNA loses its self-reparation capacity, and the cells die. The carbon beam can be more localized to the tumor area and the surrounding healthy tissue remains undamaged due to the smaller broadening of the beam. The relative biological effectiveness (RBE) is increased by two to three times when compared to the proton beam and the macroscopic dose can be reduced [53–56]. The energy-loss curve for a C beam passing through water has two important regions of interest for the energy-deposition mechanism: The maximum and the distal region of the Bragg peak. For both cases the energy range and average charge state are, respectively, 200–300 keV/u with $\bar{q}' = 2$, and 10–200 keV/u with $\bar{q}' = 1$ [4].

To investigate the angular dependence of the emission of the fragments ions, the collision of C^+ on water at an incident energy of 2 MeV was chosen (distal region of the Bragg peak) and the results are shown in Fig. 7. Figure 7(a) presents the CE-CTMC calculation and Fig. 7(b) shows the experimental data taken at the observation angles in the range 10 to 170 degrees relative to the incident-beam direction. In Fig. 7(b), the distribution with the highest intensity corresponds to a detection angle of 10 degrees and the following angles are associated with the ascending angles of 20, 30, 48, 90, 130, and 170 degrees. Note that the distributions are divided by multiples of two in order to separate them in the figure. As observed for the lithium-projectile case, the calculation shown in Fig. 7(a) suggest that the higher-energy H^+ fragments of Fig. 7(b) correspond also to the n-fold removal of electrons from the water molecule, leading to oxygen ions with charge states up to 3+.

The measured spectra do not show any significant angular dependence, indicating that the energy distribution can be considered isotropic, at least in the intermediate-energy range. This result is also predicted by the CE-CTMC calculations, as shown in Fig. 7(a). However, these results are in contrast with the strong anisotropy observed in the H^+ fragment emission induced by impact of slow, highly charged 1–50 keV Xe^{22+} [16,18], 2 keV Ne^{9+} [18], and fast 5.9 MeV/u $Xe^{q'+}$ ions [32]. They found a significant forward-backward asymmetry of the energy and intensity of the H^+ fragments. Again, it is important to point out that the above-cited experiments were

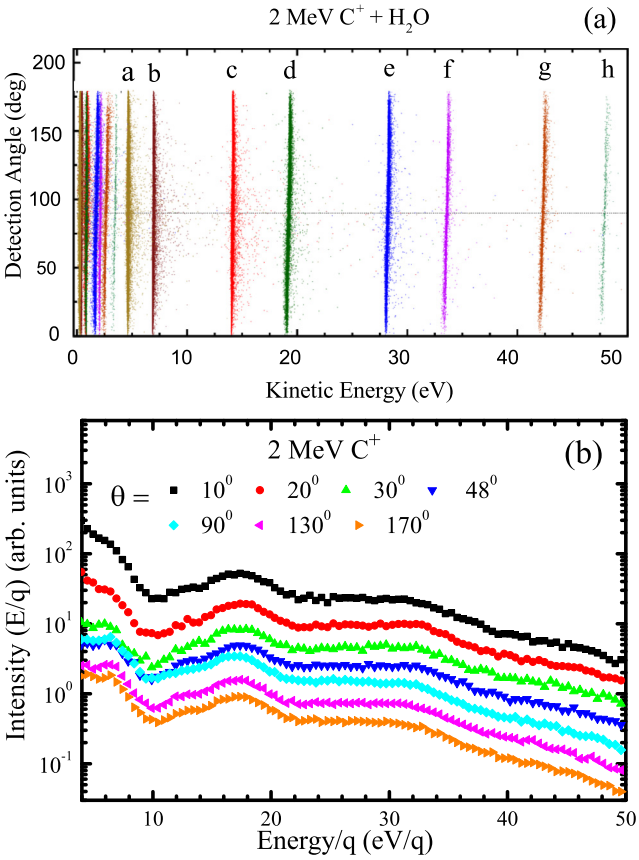

FIG. 7. (a) CE-CTMC calculations for the collision system of 2.0 MeV C^+ on H_2O. The figure represents the detection angles as function of the kinetic energies of the fragment-ion channels. The designation of fragmentation channels are also included. (b) Experimental angular distributions for 2 MeV C^+ on H_2O. Intensities at 10, 20, 30, 48, 90 130, and 170 degrees divided by 1, 2, 4, 8, 16, 32, and 64, respectively.

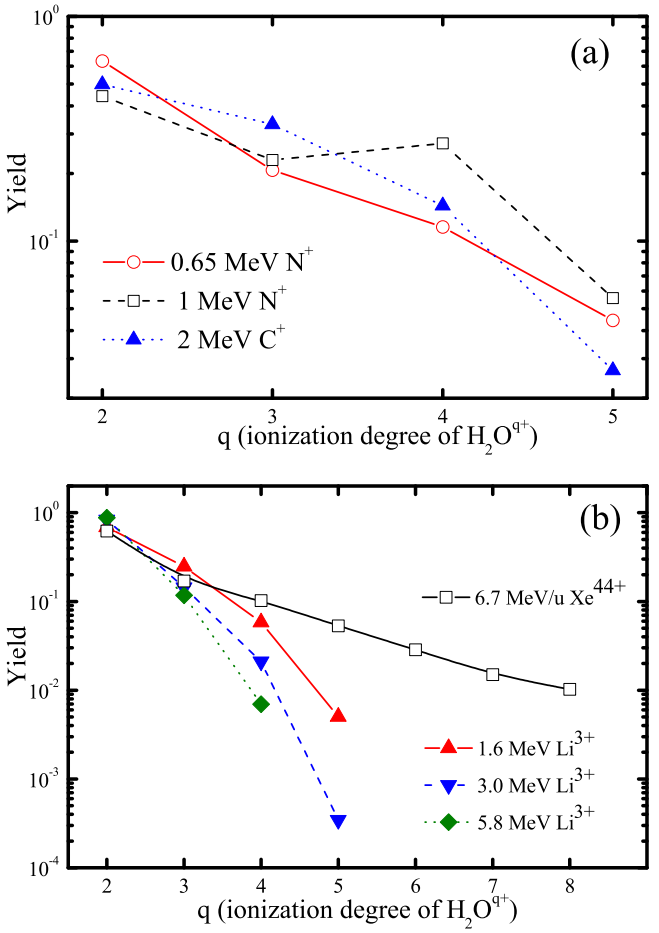

FIG. 8. Yield of multiple ionization of H_2O^{q+} ($q \geqslant 2$) normalized to the sum of multiple ionization processes ($2 \leqslant q \leqslant 5$) as a function of the ionization degree q for different projectiles. (a) Singly ionized projectiles, 0.65 MeV N^+ (red open circles) [27], 1 MeV N^+ (black open squares) [26], and 2 MeV C^+ at 10 degrees (blue closed triangles, present work). (b) Li^{3+} (present work) and Xe^{44+} [3]. 1.6 MeV Li^{3+} (red closed upward triangles), 3.0 MeV Li^{3+} (blue closed downward triangles), 5.8 MeV Li^{3+} (green closed diamonds), and 6.7 MeV/u Xe^{44+} (black open squares). Lines are to guide the eye.

carried out in a projectile-velocity regime different from that of our work and at which the PCI would play a major role.

Figure 8(a) compares the yield dependence with the ionization degree of water for singly charged nitrogen projectiles at energies of 0.65 and 1 MeV [26,27] and 2 MeV C^+ projectiles (present work). In this comparison, for example, the 3+ ionization means the sum of charges for the fragmentation channels ($H^+ + H^+ + O^+$) and ($H^+ + H + O^{2+}$). These results provide evidence that, although these projectiles are singly charged, they cause multiple ionization of water.

For these collision systems, the yield decreases approximately an order of magnitude with respect to the ionization degree. On the contrary, for Li^{3+} projectiles, Fig. 8(b) shows a rather steep decrease of the yields as function of the ionization degree, being especially pronounced for O^{4+} and O^{5+} ions. Hence, for the highly energetic Li^{3+}, the contribution of higher degrees of ionization could be neglected. The yields for the 6.7 MeV/u Xe^{44+} projectile as a function of the ionization degree of water are also included in Fig. 8(b) [3]. It can be seen that, as opposed to the Li^{3+} case, it shows a less-pronounced decrease.

B. Time-of-flight mass spectroscopy results

The time-of-flight analysis of the ionized target fragments was performed for a preset energy per charge, to overcome the limited information extracted from the energy distributions in the low-energy part of the spectra, below 6 eV, as described in Sec. II (see Fig. 2). All measurements were taken at a detection angle of 10 degrees. The relative fraction of fragments f^+ (H^+ and O^{q+}, with $q = 1$ up to 5) are extracted from the measured time-of-flight spectra for 2 MeV C^{1+} and C^{2+} on H_2O. The results are shown in Fig. 9(a) and are normalized to the total fragment-ion production. The relative fraction for the ion fragments are quite similar for both projectiles as a function of the fragment-ion energy per charge state (E/q). Highly charged oxygen ions are produced for both C^+ and C^{2+} projectiles incident with 2 MeV. The fractions as a function of the fragment-ion energy per charge for both C^+ and C^{2+} projectiles are very similar, indicating that, at least in this

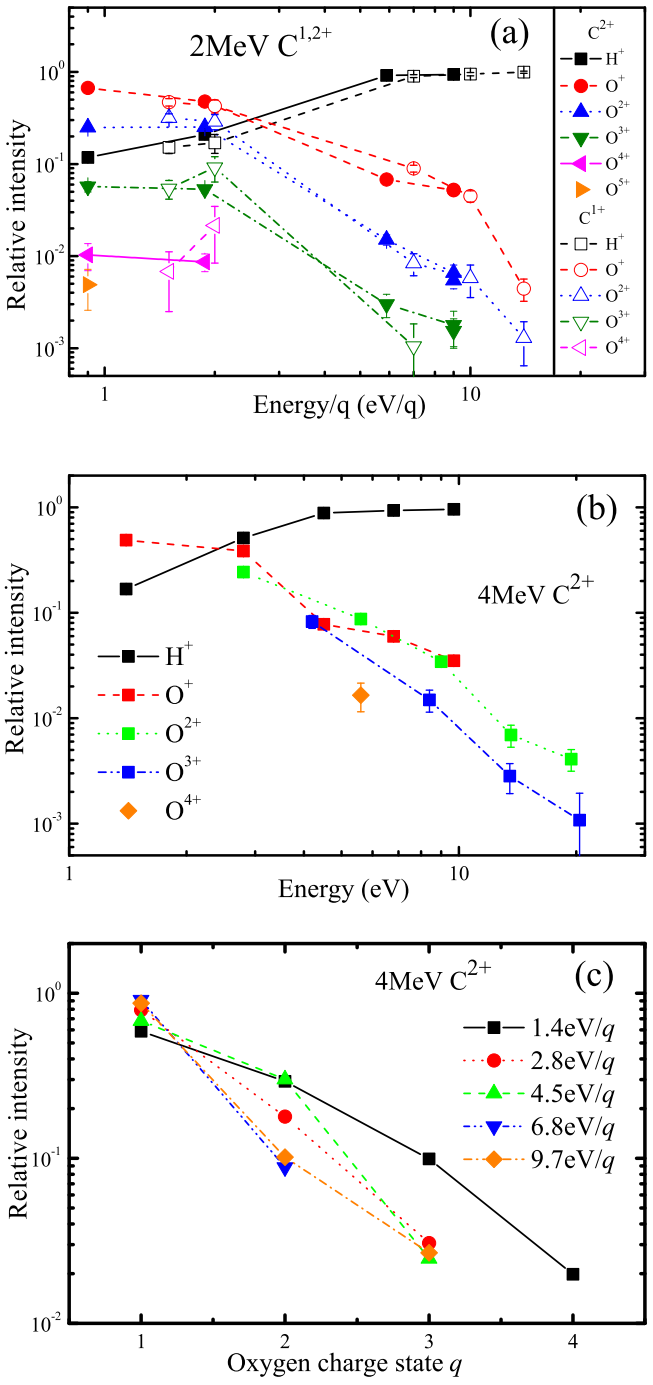

FIG. 9. (a) Relative intensities of fragment ion f^+ normalized to the sum of all charged ions differential to the selected kinetic energy of the ions in eV per charge q produced by 2 MeV C^+ and C^{2+} projectiles, C^+ (open symbols), C^{2+} (closed symbols). (b) Relative intensities of fragment ion f^+ as a function of the fragment kinetic energy, H^+ (black closed squares), O^+ (red closed circles), O^{2+} (green closed upward triangles), O^{3+} (blue closed downward triangle), O^{4+} (orange closed diamonds). (c) Relative intensity of oxygen-ion-fragment production, with $q = 1$ to 4+, normalized to the sum of all oxygen fragments. The symbols indicate the fixed energies of the fragment ions in eV per charge q, 1.4 eV/q (black solid squares), 2.8 eV/q (red solid circles), 4.5 eV/q (green solid upward triangles), 6.8 eV/q (blue solid downward triangles), and 9.7 eV/q (orange solid diamonds).

energy range, the projectile charge states do not have a major influence on the energy transferred to the O^{q+} ion fragment.

Although the expected energy to find charged oxygen was around 5 eV, some oxygen ions were collected at higher energies, despite their low relative abundance. Figure 9(b) shows the relative intensities, defined in Fig. 9(a) for the fragments H^+ and O^{q+} formed in 4 MeV C^{2+} collisions, as a function of the fragment kinetic energy. There, kinetic energies up to 10, 12, and 14 eV were found for O^+, O^{2+}, and O^{3+}, respectively.

The CE-CTMC model predicts charged oxygens ions at low kinetic energies [Fig. 7(a)]. In order to estimate the relative contribution of the oxygen ions with respect to the fragments ions energy per charge (E/q), the relative intensities of the oxygen fragments to the sum of all oxygen ions are shown in Fig. 9(c). The ion charges labeled from $q = 1$–4 represent the charge state of the oxygen ions, O^{q+}. In measurements of E/q within 1.4 to 9.7 eV/q, the main oxygen contribution comes from singly charged oxygen ions, O^+. Decreasing the probed E/q, higher charged states of oxygen ions are produced.

Comparing our results with previous experiments for low-energy, 23 keV H^+, He^+, and He^{2+} projectiles, the energy distribution of channel ($H^+ + OH^+$) shows structures for H^+ fragments peaking at 3.6, 3.9, and 5.3 eV, with their distribution extending up to 15 eV [12]. The associated OH^+ fragments, on the other hand, have peaks occurring at lower energies of 0.2, 0.21, and 0.34 eV, with their high-energy edge extending up to 1.5 eV. In the case of the channel ($H^+ + H + O^+$), the kinetic energies of H^+ and O^+ are centered around 15 and 0.3 eV, respectively. The O^+ distribution extends up to 3 eV. For faster projectiles, H^+, He^+ (100–350 keV) [31], 5.9 MeV/u $Xe^{q'+}$ [32], and 11.7 MeV/u Ni^{25+}, the studies show total fragment-energy distributions originating from double and triple ionization [30,32,33].

V. CONCLUSION

A systematic experimental and theoretical study is presented for the energy, angular distribution, and time-of-flight of fragment ions from H_2O dissociation produced in collisions with proton, lithium atom, lithium, and carbon ions at the intermediate-energy range. The fragment-ion energy distribution of water molecule shows a clear dependence in the production of higher-energy H^+ fragments (above 25 eV structure) with projectile parameters such as incident energy and charge state.

With the aid of CE-CTMC calculation these high-energy H^+ fragments were correlated with the fragmentation channels involving multiple target ionization. The calculations predict that, for the present collision systems, ionization processes arise from collisions involving small impact parameters ($b <$ 2 a.u.). Such close collisions lead to multiple ionization, which can be directly related to the O^{q+} production. In addition, it is important to note that the present CE-CTMC model inherently includes the postcollisional effects, due to the projectile field. Although they have not shown to be relevant for the present study due to the large impact energies considered, the capabilities of the model should be further explored at lower impact energies.

The findings obtained in this work are consistent with the experimental data of Refs. [50,51]. There, the occurrence of higher ionization degrees in the fragmented H_2O molecule occurs as the projectile energy decreases in the MeV/u to keV/u range. In this energy range, transfer ionization leads to H_2O^{q+} with degrees of ionization of 2+ to 4+. This becomes as important as single direct ionization and single electron capture. For higher impact energies, direct ionization prevails and higher charge states of the fragmented molecule become less abundant.

Finally, the combined experimental and theoretical study presented in this work allowed us to compare the molecular ionization followed by fragmentation with the final fast H^+ fragment energy distribution. Because of the energy range selected, the present work is relevant to applications such as hadron-therapy in cancer treatment.

ACKNOWLEDGMENTS

W.W. wishes to thank the Experimental Group of Divisiones Atómicas of the Centro Atómico Bariloche to the opportunity to measure at the Pelletron accelerator. Brazilian agencies, Fundação Carlos Chagas Filho de Amparo à Pesquisa do Estado do Rio de Janeiro and Conselho Nacional de Desenvolvimento Científico e Tecnológico, are gratefully acknowledged. Work at IFISUR supported by Grants No. PGI 24/F059 (Universidad Nacional del Sur–(Argentina)) and No. PIP 112-201101-00749 of CONICET-Argentina. R.S. acknowledges the support by the EU through FP7PEOPLE-2010-IRSES, program 269243 DWBQS.

[1] *Radiation Chemistry: Principles and Applications*, edited by Farhataziz and M. A. J. Rodgers (VCH Publishers, New York, 1987).

[2] *Charged Particle and Photon Interactions with Matter*, edited by Y. Hatano, Y. Katsumura, and A. Mozumder (CRC Press Taylor and Francis Group, Boca Raton, 2011), Chap. 14, pp. 326–354.

[3] G. H. Olivera, C. Caraby, P. Jardin, A. Cassimi, L. Adoui, and B. Gervais, Multiple ionization in the earlier stages of water radiolysis, Phys. Med. Biol. **43**, 2347 (1998), and references therein.

[4] E. C. Montenegro, M. B. Shah, H. Luna, S. W. J. Scully, A. L. F. de Barros, J. A. Wyer, and J. Lecointre, Water Fragmentation and Energy Loss by Carbon Ions at the Distal Region of the Bragg Peak, Phys. Rev. Lett. **99**, 213201 (2007).

[5] B. Gervais, M. Beuve, G. H. Olivera, M. E. Galassi, and R. D. Rivarola, Production of H_2 O and O_2 by multiple ionization in water radiolysis by swift carbon ions, Chem. Phys. Lett. **410**, 330 (2005).

[6] B. Gervais, M. Beuve, G. H. Olivera, and M. E. Galassi, Numerical simulation of multiple ionization and high LET effects in liquid water radiolysis, Radiat. Phys. Chem. **75**, 493 (2006).

[7] C. Champion, Multiple ionization of water by heavy ions: A Monte Carlo approach, Nucl. Instrum. Methods Phys. Res., Sect. B **205**, 671 (2003).

[8] C. Champion, A. L'Hoir, M. F. Politis, P. D. Fainstein, R. D. Rivarola, and A. Chetioui, A Monte Carlo code for the simulation of heavy-ion tracks in water, Radiat. Res. **163**, 222 (2005).

[9] D. S. Gemmel, Determining the stereo-chemical structures of molecular ions by "Coulomb-explosion" techniques with fast (MeV) molecular ion beams, Chem. Rev. (Washington, DC, U. S.) **80**, 301 (1980).

[10] C. J. Latimer, The dissociative ionization of simple molecules by fast ions, Adv. At. Mol. Phys. **30**, 105 (1993).

[11] N. Stolterfoht, R. Cabrera-Trujillo, R. Hellhammer, Z. Pešic, E. Deumens, Y. Öhrn, and J. R. Sabin, Charge exchange and fragmentation in slow collisions of He^{2+} with water molecules, Adv. Quantum Chem. **52**, 149 (2007).

[12] F. Alvarado, R. Hoekstra, and T. Schlathölter, Dissociation of water molecules upon keV H^+- and He^{q+}-induced ionization, J. Phys. B: At., Mol. Opt. Phys. **38**, 4085 (2005).

[13] P. Sobocinski, Z. D. Pešic, R. Hellhammer, N. Stolterfoht, J.-Y. Chesnel, S. Legendre, and B. Sulik, Fragmentation of H_2 O molecules following interaction with slow He^{2+} ions, Nucl. Instrum. Methods Phys. Res., Sect. B **233**, 207 (2005).

[14] P. Sobocinski, Z. D. Pešic, R. Hellhammer, N. Stolterfoht, B. Sulik, S. Legendre, and J.-Y. Chesnel, Fragmentation of water molecules in slow He^{2+} + H_2 O collisions, J. Phys. B: At., Mol. Opt. Phys. **38**, 2495 (2005).

[15] B. Seredyuk, R. W. McCullough, H. Tawara, H. B. Gilbody, D. Bodewits, R. Hoekstra, A. G. G. M. Tielens, P. Sobocinski, Z. D. Pešic, R. Hellhammer, B. Sulik, N. Stolterfoht, O. Abu-Haija, and E. Y. Kamber, Charge exchange and dissociative processes in collisions of slow He^{2+} ions with H_2O molecules, Phys. Rev. A **71**, 022705 (2005).

[16] P. Sobocinski, Z. D. Pešic, R. Hellhammer, D. Klein, B. Sulik, Y. D. Chesnel, and N. Stolterfoht, Anisotropic proton emission after fragmentation of H_2O by multiply charged ions, J. Phys. B: At., Mol. Opt. Phys. **39**, 927 (2006).

[17] Z. D. Pešic, J.-Y. Chesnel, R. Hellhammer, B. Sulik, and N. Stolterfoht, Fragmentation of H_2O molecules following the interaction with slow, highly charged Ne ions, J. Phys. B: At., Mol. Opt. Phys. **37**, 1405 (2004).

[18] Z. D. Pešic, R. Hellhammer, B. Sulik, and N. Stolterfoht, Strong anisotropy in the proton emission following fragmentation of H_2O molecules by impact with slow, highly charged xenon ions, J. Phys. B: At., Mol. Opt. Phys. **42**, 235202 (2009).

[19] S. Martin, L. Chen, R. Brédy, J. Bernard, and A. Cassimi, Fragmentation of doubly charged HDO, H_2O, and D_2O molecules induced by proton and monocharged fluorine beam impact at 3 keV, J. Chem. Phys. **142**, 094306 (2015).

[20] O. Abu-Haija, E. Y. Kamber, and S. M. Ferguson, Single-electron capture by He^{2+} ions from triatomic molecules, Nucl. Instrum. Methods Phys. Res., Sect. B **205**, 634 (2003).

[21] H. Luna and E. C. Montenegro, Fragmentation of Water by Heavy Ions, Phys. Rev. Lett. **94**, 043201 (2005).

[22] A. C. Tavares, H. Luna, W. Wolff, and E. C. Montenegro, Double ionization of water molecules induced by swift protons, Phys. Rev. A **92**, 032714 (2015).

[23] A. L. F. de Barros, J. Lecointre, H. Luna, M. B. Shah, and E. C. Montenegro, Energy distributions of H^+ fragments ejected

by fast proton and electron projectiles in collision with H_2O molecules, Phys. Rev. A **80**, 012716 (2009).

[24] F. Gobet, B. Farizon, M. Farizon, M. J. Gaillard, M. Carré, M. Lezius, P. Scheier, and T. D. Mark, Total, Partial, and Electron-Capture Cross Sections for Ionization of Water Vapor by 20–150 keV Protons, Phys. Rev. Lett. **86**, 3751 (2001).

[25] F. Gobet, S. Eden, B. Coupier, J. Tabat, B. Farizon, M. Farizon, M. J. Gaillard, M. Carré, S. Ouaskit, T. D. Mark *et al.*, Ionization of water by (20—-150)-keV protons: Separation of direct-ionization and electron-capture processes, Phys. Rev. A **70**, 062716 (2004).

[26] S. T. S. Kovács, Z. Huhász, P. Herczku, and B. Sulik, A new setup for molecules fragmentation studies and the first results from $N^+ + H_2O$ collisions, Acta Phys. Debrecina **XLVI**, 65 (2012).

[27] S. T. S. Kovács, P. Herczku, and B. Sulik, Fragmentation of H_2O and CH_4 molecules induced by 650 keV N^+ projectiles, Acta Phys. Debrecina **XLVII**, 87 (2013).

[28] J. Rajput and C. P. Safvan, Atomic and molecular Rydbergs from water, J. Chem. Phys. **134**, 201101 (2011).

[29] J. Rajput and C. P. Safvan, Fragmentation of water by ion impact: Kinetic energy release spectra, Phys. Rev. A **84**, 052704 (2011).

[30] U. Werner, K. Beckord, J. Becker, H. O. Folkerts, and H. O. Lutz, Ion-impact-induced fragmentation of water molecules, Nucl. Instrum. Methods Phys. Res., Sect. B **98**, 385 (1995).

[31] U. Werner, K. Beckord, J. Becker, and H. O. Lutz, 3D imaging of the collision-induced Coulomb fragmentation of water molecules, Phys. Rev. Lett. **74**, 1962 (1995).

[32] B. Siegmann, U. Werner, H. O. Lutz, and R. Mann, Multiple ionization and fragmentation of H_2O in collision with fast highly charged Xe ions, J. Phys. B: At., Mol. Opt. Phys. **34**, L587 (2000).

[33] S. Legendre, E. Giglio, M. Tarisien, A. Cassimi, B. Gervais, and L. Adoui, Isotopic effects in water dication fragmentation, J. Phys. B: At., Mol. Opt. Phys. **38**, L233 (2005).

[34] J. R. Sabin, R. Cabrerra-Trujillo, N. Stolterfoht, E. Deumens, and Y. Öhrn, Fragmentation of water on swift He^{2+} ion impact, Nucl. Instrum. Methods Phys. Res., Sect. B **267**, 196 (2009).

[35] J. Severs, F. Harris, S. Andrews, and D. Parry, Triplet-state energies of H_2O^{2+}: A combined experimental and theoretical study, Chem. Phys. **175**, 467 (1993).

[36] S. Limandri, C. Olivares, L. Rodriguez, G. Bernardi, and S. Suárez, PIXE facility at Centro Atómico Bariloche, Nucl. Instrum. Methods Phys. Res., Sect. B **318**, 47 (2014).

[37] G. Bernardi, S. Suárez, D. Fregenal, P. Focke, and W. Meckbach, Measurement of doubly differential electron distributions induced by atomic collisions: Apparatus and related instrumental effects, Rev. Sci. Instrum. **67**, 1761 (1996).

[38] S. Martínez, G. Bernardi, P. Focke, A. D. González, and S. Suárez, H_2 dissociation by H^+ and He^{2+} projectiles at intermediate energies, J. Phys. B: At., Mol. Opt. Phys. **36**, 4813 (2003).

[39] F. B. Yousif, B. G. Lindsay, and C. J. Latimer, The double ionisation of hydrogen by 5–30 keV protons, J. Phys. B: At., Mol. Opt. Phys. **21**, 4157 (2003).

[40] P. Sobocinski, J. Rangama, G. Laurent, L. Adoui, A. Cassimi, J.-Y. Chesnel, A. Dubois, D. Hennecarrt, X. Husson, and F. Frémont, Evidence for highly energetic fragments following electron capture in $O^{5+} + H_2$ collisions at low impact velocities, J. Phys. B: At. Mol. Opt. Phys. **35**, 1353 (2002).

[41] M. Tarisien, L. Adoui, F. Frémont, D. Lelièvre, L. Guillaume, J-Y. Chesnel, H. Zhang, A. Dubois, D. Mathur, Sanjay Kumar, M. Krishnamurthy, and A. Cassimi, Ion-induced molecular fragmentation: Beyond the Coulomb explosion picture, J. Phys. B: At., Mol. Opt. Phys. **33**, L11 (2000).

[42] L. Adoui, C. Caraby, A. Cassimi, D. Lelièvre, J. P. Grandin, and A. Dubois, Fast ion-induced Co molecules fragmentation in the strong interaction regime, J. Phys. B: At., Mol. Opt. Phys. **32**, 631 (1999).

[43] U. Werner, B. Siegmann, H. Lebius, B. Huber, and H. O. Lutz, Multiple ionization and fragmentation of CH_4 in collision with slow highly charged ion, Nucl. Instrum. Methods Phys. Res., Sect. B **205**, 639 (2003).

[44] J.-Y. Chesnel, Z. Juhász, E. Lattouf, J. A. Tanis, B. A. Huber, E. Bene, S. T. S. Kovács, P. Herczku, A. Méry, J.-C. Poully, J. Rangama, and B. Sulik, Anion emission from water molecules colliding with positive ions: Identification of binary and many-body processes, Phys. Rev. A **91**, 060701(R) (2015).

[45] R. E. Olson and A. Salop, Charge-transfer and impact-ionization cross sections for fully and partially stripped positive ions colliding with atomic hydrogen, Phys. Rev. A **16**, 531 (1977).

[46] R. H. Garvey, C. H. Jackman, and A. E. S. Green, Independent-particle-model potentials for atoms and ions with $36 < Z \leqslant 54$ and a modified Thomas-Fermi atomic energy formula, Phys. Rev. A **12**, 1144 (1975).

[47] S. Hsie and J. H. D. Eland, Charge separation reaction dynamics from pepipico using a position-sensitive detector, Rapid Commun. Mass Spectrom. **9**, 1261 (1995).

[48] Z. D. Pešic, D. Rolles, R. C. Bilodeau, I. Dimitriu, and N. Berrah, Three-body fragmentation of CO_2^{2+} upon K-shell photoionization, Phys. Rev. A **78**, 051401 (2008).

[49] H. Sann, T. Jahnke, T. Havermeier, K. Kreidi, C. Stuck, M. Meckel, M. S. Schöffler, N. Neumann, R. Wallauer, S. Voss, A. Czasch, O. Jagutzki, Th. Weber, H. Schmidt-Böcking, S. Miyabe, D. J. Haxton, A. E. Orel, T. N. Rescigno, and R. Dörner, Electron diffraction self-imaging of molecular fragmentation in two-step double ionization of water, Phys. Rev. Lett. **106**, 133001 (2011).

[50] J. S. Ihani, H. Luna, W. Wolff, and E. C. Montenegro, Multiple Ionization of neon induced by Li^{3+} and C^{3+} projectiles: Influence of projectile screening in the ionization and electron-capture channels, J. Phys. B: At. Mol. Opt. Phys. **46**, 115208 (2013).

[51] H. Luna, W. Wolff, A. C. Tavares, E. C. Montenegro, H. J. Ludde, G. Schenk, M. Horbatsch, and T. Kirchner, Ionization and electron-capture cross sections for single- and multiple-electron removal from H_2O by Li^{3+} impact, Phys. Rev. A **93**, 052705 (2016).

[52] V. Marx, Cancer treatment: Sharp shooters, Nature (London) **508**, 133 (2014).

[53] T. Ohno, Particle radiotherapy with carbon ion beams, EPMA J. **4**:9 (2013).

[54] A. Degiovanni and U. Amaldi, History of hadron therapy accelerators, Phys. Med. **31**, 322 (2015).

[55] L. Antonovic, A. Dasu, Y. Furusawa, and I. Toma-Dasu, Relative clinical effectiveness of carbon ion radiotherapy: Theoretical modeling for HN tumors, J. Radiat. Res. **56**, 639 (2015).

[56] D. Schardt, T. Elsässer, and D. Schulz-Ertner, Heavy-ion tumor therapy: Physical and radiobiological benefits, Rev. Mod. Phys. **82**, 383 (2010).